31034 photomultiplier tube followed by a photon-count processing system. The spectra were recorded at ambient temperatures by making pressed pellets of the compounds. Magnetic susceptibilities were measured by the Gouy method by using $Hg[Co(NCS)_4]$ as the calibrant. ESR spectra of the solids as well as of aqueous solutions of the compounds were recorded by using a Varian E109, X-band ESR spectrometer with 100-K_c field modulator. Molar conductance measurements were made by using a Philips PR 9500 conductivity bridge. Conductivity grade water was used for the purpose. pH values of the reaction solutions were measured by using a Systronics Type 335 digital pH meter and also by BDH indicator paper.

Elemental analyses were performed following the methods described in our earlier papers.[33,40]

Reaction of Alkali-Metal Triperoxyvanadate(V) Trihydrates, $A[V(O_2)_3]\cdot 3H_2O$ (A = Na, K), with SO_2(g). (a) Isolation of Yellow Potassium Aquaoxodiperoxyvanadate(V), $K[VO(O_2)_2(H_2O)]$. The deep blue microcrystalline $K[V(O_2)_3]\cdot 3H_2O$ (1.5 g; 6.25 mmol) was dissolved in 10 cm^3 of water. SO_2(g) was slowly bubbled through the blue solution with occasional shaking until the solution attained a uniform yellow color and deposited a yellow microcrystalline product. The pH of the solution at this stage was ca. 6. The compound was separated by filtration, washed repeatedly with ethanol, and finally dried in vacuo over concentrated H_2SO_4.

The yield of the compound was 0.8 g (70%). Anal. Calcd for $K[VO(O_2)_2(H_2O)]$: K, 20.74; V, 27.13; peroxide (O_2^{2-}), 34.04. Found: K, 20.33; V, 26.92; peroxide (O_2^{2-}), 33.88.

(b) Isolation of Blue Alkali-Metal Triaquabis(sulfato)oxovanadate(IV) Monohydrates, $A_2[VO(SO_4)_2(H_2O)_3]\cdot H_2O$ (A = Na, K). $A[V(O_2)_3]\cdot 3H_2O$ (6.6 mmol) was dissolved in 10 cm^3 of water. Bubbling of SO_2(g) through this solution resulted in different color changes. First, the solution changes color from deep blue to yellow, then to deep green, and ultimately to green-blue and does not undergo anymore change on further bubbling of SO_2(g) (in the case of the reaction of $K[V(O_2)_3]\cdot 3H_2O$ with SO_2 a yellow microcrystalline solid precipitated from the yellow solution, which redissolved on further bubbling of SO_2). The pH of the solution at this stage was recorded to be ca. 2. Bubbling of SO_2(g) was stopped and the solution filtered to remove any undissolved residue. To the clear solution was slowly added ethanol until a blue oily mass was formed. Addition of an excess of ethanol is detrimental as this contaminates the product with white alkali-metal sulfate, A_2SO_4. The blue oily mass was separated by decantation, treated several times with an ethanol-acetone (1:1) mixture, and finally dried in vacuo over concentrated H_2SO_4 to afford blue solid $A_2[VO(SO_4)_2(H_2O)_3]\cdot H_2O$.

The yields of $Na_2[VO(SO_4)_2(H_2O)_3]\cdot H_2O$ and $K_2[VO(SO_4)_2(H_2O)_3]\cdot H_2O$ were 1.2 g (48%) and 1.3 g (51%), respectively. Anal. Calcd for $K_2[VO(SO_4)_2(H_2O)_3]\cdot H_2O$: K, 19.07; V, 12.46; SO_4^{2-}, 46.94. Found: K, 18.87; V, 12.12; SO_4^{2-}, 47.3. Calcd for $Na_2[VO(SO_4)_2(H_2O)_3]\cdot H_2O$: Na, 12.20; V, 13.52; SO_4^{2-}, 50.92. Found: Na, 12.36; V, 13.24; SO_4^{2-} 51.18.

The reaction was monitored by ESR spectrometry. Whereas the deep blue solution of $A[V(O_2)_3]\cdot 3H_2O$ was completely ESR silent, as expected, the ultimate green-blue solution, obtained through SO_2(g) reaction, was ESR active, giving characteristic signals of vanadium(IV). It is also important to mention that the yellow solution obtained at an intermediate stage of color changes was ESR inactive.

Reactions of $A[V(O_2)_3]\cdot 3H_2O$ (A = Na, K) with SO_2(g) in the Presence of AF (A = Na, K) and Synthesis of Ternary Complex Alkali-Metal Aquabis(sulfato)difluorooxovanadate(IV) Dihydrates, $A_4[VO(SO_4)_2F_2(H_2O)]\cdot 2H_2O$ (A = Na, K). $A[V(O_2)_3]\cdot 3H_2O$ (6.6 mmol) and AF (13.3 mmol) were dissolved in about 15 cm^3 of water, maintaining the atom ratio of V:F at 1:2. SO_2(g) was bubbled through this solution in a manner similar to that described under the preceding reaction. The color changes were also similar to those observed therein. Here again, the ultimate green-blue solution was found to be ESR active (cf. vanadium(IV)). The green-blue solution was worked up in an analogous manner as described earlier for the isolation of $A_2[VO(SO_4)_2(H_2O)_3]\cdot H_2O$ (polyethylene apparatus was used in this reaction). The products obtained in the present reaction have been analyzed as blue $A_4[VO(SO_4)_2F_2(H_2O)]\cdot 2H_2O$. The yields of $Na_4[VO(SO_4)_2F_2(H_2O)]\cdot 2H_2O$ and $K_4[VO(SO_4)_2F_2(H_2O)]\cdot 2H_2O$ were 1.5 g (52%) and 1.6 g (49%), respectively.

Anal. Calcd for $K_4[VO(SO_4)_2F_2(H_2O)]\cdot 2H_2O$: K, 30.76; V, 10.06; SO_4^{2-}, 37.86; F^-, 7.49. Found: K, 31.07; V, 9.89; SO_4^{2-}, 37.21; F^-, 7.63. Calcd. for $Na_4[VO(SO_4)_2F_2(H_2O)]\cdot 2H_2O$: Na, 20.76; V, 11.51; SO_4^{2-}, 43.34; F^-, 8.57. Found: Na, 20.39; V, 11.43; SO_4^{2-}, 43.81; F^-, 8.61.

Acknowledgment. We thank the Council of Scientific and Industrial Research, New Delhi, India, for the award of a research fellowship to N.S.I.

Registry No. $Na[V(O_2)_3]$, 96760-79-1; $K[V(O_2)_3]$, 96760-80-4; SO_2, 7446-09-5; $K[VO(O_2)_2(H_2O)]$, 74994-34-6; $Na_2[VO(SO_4)_2(H_2O)_3]\cdot H_2O$, 120544-91-4; $K_2[VO(SO_4)_2(H_2O)_3]\cdot H_2O$, 120544-92-5; $Na_4[VO(SO_4)_2F_2(H_2O)]\cdot 2H_2O$, 120544-93-6; $K_4[VO(SO_4)_2F_2(H_2O)]\cdot 2H_2O$, 120544-94-7; H_2O_2, 7722-84-1.

Contribution from the Department of Chemistry, University of Rochester, Rochester, New York 14627

Optical versus Thermal Electron Transfer between Iridium(I) Maleonitriledithiolate Complexes and Methyl Viologen

Elise Graham Megehee, Curtis E. Johnson, and Richard Eisenberg*

Received August 3, 1988

Acetonitrile solutions of the anionic Ir(I) complexes $IrLL'(mnt)^{n-}$ [mnt = maleonitriledithiolate; n = 1, L = L' = CO, $P(OPh)_3$; n = 1, L = CO, L' = PPh_3; n = 2, L = CO, L' = CN^-] with methyl viologen (MV^{2+}) exhibit outer-sphere electron-transfer behavior ranging from optical to thermal. The type of electron-transfer behavior observed correlates with the reducing ability of the Ir(I) complexes as determined by their irreversible oxidation waves. The least reducing complex, $Ir(CO)_2(mnt)^-$, undergoes optical charge transfer with MV^{2+} while the most reducing system, $Ir(CO)(CN)(mnt)^{2-}$, reduces MV^{2+} to the $MV^{+\bullet}$ radical cation thermally. The other complexes, $Ir(CO)(PPh_3)(mnt)^-$ and $Ir(P(OPh)_3)_2(mnt)^-$, show optical CT bands with MV^{2+} and undergo photoassisted and photoinduced electron transfer, respectively. The charge-transfer ion-pair $MV[Ir(CO)_2(mnt)]_2$ crystallizes in the monoclinic space group $C2/c$ in a unit cell of dimensions a = 14.754 (4) Å, b = 10.063 (3) Å, c = 19.985 (7) Å, and β = 103.73 (3)° with Z = 4. The structure consists of square-planar Ir(I) anions and MV^{2+} cations of C_2 symmetry that are twisted by 37.8° about the C–C bond between methylpyridinium rings. The dihedral angle between the methylpyridinium ring of MV^{2+} and the nearest neighbor Ir(I) anion is 9.2° with a cation–anion separation in the range 3.2–3.6 Å. The nature of the one-electron-oxidation product for the thermal electron-transfer process was established by oxidation of $Ir(CO)(P(p\text{-tol})_3)(mnt)^-$ (p-tol = p-tolyl) using the ferrocenium cation and determination of the crystal structure of the Ir(II) product. This dark red crystalline product was determined to be $[Ir(CO)(P(p\text{-tol})_3)(mnt)]_2$ with chelating mnt ligands bridging the Ir–Ir bond. It crystallizes in the monoclinic space group $P2_1/n$ in a unit cell of dimensions a = 14.874 (8) Å, b = 17.394 (5) Å, c = 19.99 (1) Å, and β = 96.46 (5)° with Z = 4. The structure shows square-pyramidal coordination at each Ir atom and overall C_{2v} symmetry for the complex. The Ir–Ir bond length is 2.706 (2) Å. On the basis of the position of the CT band for the $Ir(P(PPh_3)_2(mnt)^-/MV^{2+}$ system, the reorganization energy for the Ir(I/II) couple in this complex is estimated to be large (40–44 kcal/mol).

Introduction

Optical-electron-transfer processes have attracted the interest of chemists for many years. Initially, this interest was stimulated by the formation of colors in solution that none of the solution components exhibited individually. More recently, optical electron transfer has been shown to be intimately related to thermal electron transfer, and the impetus to study charge-transfer systems has been provided by their relevance to testing electron-transfer

0020-1669/89/1328-2423$01.50/0

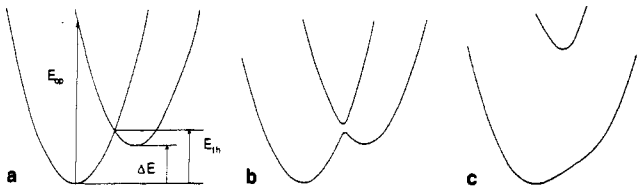

Figure 1. Potential energy diagrams for electron transfer between reactant and product surfaces for the case where $\Delta E > 0$. The extent of interaction or mixing assumed is (a) zero, (b) small, and (c) large.

theories and to the optical properties that these systems may possess.[1,2]

If thermal electron transfer in Figure 1a corresponds to crossing from the reactant surface to the product surface via the intersection at energy E_{th}, then optical charge transfer is the vertical transition from reactant to product surface denoted by E_{op}. The relationship between E_{op} and E_{th} is

$$E_{op} = \lambda + \Delta E_0 \quad (1)$$

$$E_{th} = E_{op}^2/4(E_{op} - \Delta E_0) = 0.25(E_{op} - \Delta E_0)[1 + \Delta E_0/(E_{op} - \Delta E_0)]^2 \quad (2)$$

where ΔE_0 is the driving force for the electron-transfer reaction and λ corresponds to a reorganization energy for both reactants and solvent. The transition E_{op} is generally a broad, featureless band that imparts the unusual color to charge-transfer solutions.[1]

A key aspect of electron-transfer and charge-transfer theory is the degree to which interaction or mixing occurs between reactant and product surfaces.[1-3] In Figure 1a, no mixing is assumed. If interaction or mixing is allowed to occur, then the situations shown in parts b and c of Figure 1 can arise. In Figure 1b, a small interaction exists, and the system is said to be weakly coupled; the conclusions interrelating E_{op} and E_{th} remain mainly unchanged from those of Figure 1a. For Figure 1c, however, large mixing leads to a truly delocalized electronic structure of reactants and products, and two distinct minima no longer exist on the ground-state surface.

For optical electron transfer, the most extensively studied inorganic systems are those based on mixed-valence binuclear compounds in which two redox sites are part of the same molecule.[2,4] The two sites may be the same or different, and the degree of interaction of mixing can vary widely. The well-studied Creutz–Taube complex $[(NH_3)_5Ru(pz)Ru(NH_3)_5]^{5+}$ [4a] exemplifies the delocalized limit with mixing of $\sim$3300 cm^{-1}, while the closely related ion $[(NH_3)_5Ru(4,4'\text{-bpy})Ru(NH_3)_5]^{5+}$ shows a broader, solvent-dependent E_{op} band that is analyzed in terms of weak coupling ($\sim$400 cm^{-1}).[4d] The number of mixed-valence binuclear compounds is large, and their optical-charge-transfer properties have been reviewed and discussed extensively.[2]

A far smaller class of systems showing optical-charge-transfer bands are those in which the two redox sites belong to different molecules. A considerable association of oxidant and reductant is required in these cases to see the outer-sphere optical charge transfer, and this may be facilitated by oxidant and reductant carrying charges of opposite sign.[5] For example, $Co(NH_3)_6^{3+}$ and $Ru(CN)_6^{4-}$ form an association complex that exhibits a solvent-dependent optical charge transfer.[6] One of the better studied outer-sphere charge-transfer systems is that of $MV^{2+}/Fe(CN)_6^{2-}$ (MV^{2+} = methyl viologen).[7] Meyer and co-workers have analyzed this system by using the intensity and position of E_{op} and have correlated the results with Marcus theory using self-exchange rate constants.[7c] Much more intense outer-sphere charge-transfer bands have been obtained by Vogler in solutions of square-planar complexes of opposite sign, notably $Ni(tim)^{2+}$ (tim = tetramethyl-1,4,8,11-tetraazatetradecatetraene) and $M(mnt)_2^{2-}$ (M = Ni, Pd, Pt; mnt = maleonitriledithiolate).[8] In these systems, however, no net chemistry is observed to occur.

According to Mulliken,[9] CT excitation of weakly associated electron-donor–acceptor complexes creates a strong oxidant and a strong reductant within the same complex. Recently, Kochi and co-workers have carried out a series of studies on charge-transfer-complex formation and chemistry between substituted anthracenes and the electron acceptors TCNE and tetranitromethane (TNM).[10] The association constants for these CT complexes are relatively small ($\sim 10^2$) as are their molar absorptivities ($\epsilon \sim 250$ M^{-1} cm^{-1}), but the quantum yields for photoreaction between the substituted anthracenes and TNM using the CT bands were found to be very high ($\sim$0.7), indicating that net chemistry can result by irradiating into outer-sphere charge-transfer transitions. A key to the success of this chemistry is a rapid and irreversible reaction of one of the components of the CT complex, which competes effectively with the unproductive back-reaction.[10]

In 1983, we reported the synthesis and characterization of a series of d^8 square-planar complexes of general formula $MLL'(mnt)^{n-}$ (mnt = maleonitriledithiolate):[11]

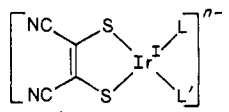

1: L = L' = CO; $n = 1$
2: L = L' = $P(OPh)_3$; $n = 1$
3: L = CO; L' = PPh_3; $n = 1$
4: L = CO; L' = CN; $n = 2$

These complexes were found to luminesce brightly in rigid media, and studies of their emission properties as a function of ligand L led to the conclusion that the emitting state for these complexes was a metal-to-ligand charge transfer (MLCT) of d–π^*(mnt) character. The emitting-state lifetimes ranged from 10 to 300 μs depending on the metal. Further study showed that while the emission was maintained at 25 °C in rigid media such as polycarbonate (Lexan), it was quenched in fluid solution, even at −78 °C.

In the course of examining the possible photochemistry of the anionic complexes $IrLL'(mnt)^-$, solutions were prepared that contained MV^{2+}. Surprisingly, some of the solutions showed weak intermolecular charge-transfer bands while others exhibited evidence of thermal electron transfer. This paper outlines a detailed investigation of the $IrLL'(mnt)^-/MV^{2+}$ system which shows that by simple variation of L and L' the reducing ability of the d^8 complex changes, leading to different types of electron-transfer behavior including photoassisted and photopromoted electron transfer. The structure of the charge-transfer salt $MV[Ir(CO)_2(mnt)]_2$ has also been determined crystallographically, as has the structure of an Ir(II) dimer produced by one-electron oxidation of $Ir(CO)(P(p\text{-tol})_3)(mnt)^-$ (p-tol = p-tolyl).

(1) (a) Allen, G. C.; Hush, N. S. *Prog. Inorg. Chem.* **1961**, *8*, 357. (b) Hush, N. S. *Prog. Inorg. Chem.* **1961**, *8*, 391.
(2) (a) Brown, D. B., Ed. *Mixed-Valence Compounds*; Reidel Publishing Co.: Dordrecht, Holland, 1980 and references therein. (b) Creutz, C. *Prog. Inorg. Chem.* **1983**, *30*, 1. (c) Meyer, T. J. *Acc. Chem. Res.* **1978**, *11*, 94. (d) Meyer, T. J. *Prog. Inorg. Chem.* **1983**, *30*, 389 and references therein.
(3) Robin, M. B.; Day, P. *Adv. Inorg. Chem. Radiochem.* **1967**, *10*, 247.
(4) (a) Creutz, C.; Taube, H. *J. Am. Chem. Soc.* **1969**, *91*, 3988. (b) Toma, H. J. *J. Chem. Soc., Dalton Trans.* **1980**, *3*, 471. (c) Curtis, J. C.; Meyer, T. J. *J. Am. Chem. Soc.* **1978**, *100*, 6284. (d) Tom, G. M.; Creutz, C.; Taube, H. *J. Am. Chem. Soc.* **1974**, *96*, 7828.
(5) Vogler, A.; Osman, A. H.; Kunkely, H. *Coord. Chem. Rev.* **1985**, *64*, 159.
(6) Vogler, A.; Kisslinger, J. *Angew. Chem., Int. Ed. Engl.* **1982**, *21*, 77.
(7) (a) Nakahara, A.; Wang, J. H. *J. Phys. Chem.* **1963**, *67*, 496. (b) Toma, H. E. *Can. J. Chem.* **1979**, *57*, 2079. (c) Curtis, J. C.; Sullivan, B. P.; Meyer, T. J. *Inorg. Chem.* **1980**, *19*, 3833.
(8) Vogler, A.; Kunkely, H. *J. Chem. Soc., Chem. Commun.* **1986**, 1616.
(9) (a) Mulliken, R. S. *J. Am. Chem. Soc.* **1952**, *74*, 811. (b) Mulliken, R. S.; Person, W. B. *Molecular Complexes: A Lecture and Reprint Volume*; Wiley-Interscience: New York, 1969.
(10) (a) Masnovi, J. M.; Kochi, J. K.; Hilinski, E. F.; Rentzepis, P. M. *J. Am. Chem. Soc.* **1986**, *108*, 1126. (b) Hilinski, E. F., Masnovi, J. M.; Kochi, J. K.; Rentzepis, P. M. *J. Am. Chem. Soc.* **1984**, *106*, 8071.
(11) Johnson, C. E.; Eisenberg, R.; Evans, T. R.; Burberry, M. S. *J. Am. Chem. Soc.* **1983**, *105*, 1795.

Experimental Section

Materials. The following compounds were used as received: iridium trichloride hydrate (Johnson Matthey), triphenylphosphine, triphenyl phosphite, tetra-*n*-butylammonium (TBA^+) bromide, ammonium hexafluorophosphate, methyl viologen (MV^{2+}) dichloride dihydrate (Aldrich), tetra-*n*-butylammonium cyanide (Fluka), tri-*p*-tolylphosphine (Strem). Sodium maleonitriledithiolate (Na_2mnt)[12] and ferrocenium hexafluorophosphate ($FcPF_6$)[13] were prepared according to literature methods. Reagent grade solvents were used for synthesis. For spectroscopic studies acetonitrile (Baker HPLC) was dried over P_2O_5 and distilled under nitrogen immediately prior to use.

Preparation of Complexes. The preparation of the complexes TBA[$Ir(CO)_2(mnt)$], TBA[$Ir(CO)(PR_3)(mnt)$] (R = phenyl, *p*-tolyl) and TBA[$Ir(P(OPh)_3)_2(mnt)$] has been previously described.[11,14] All syntheses were performed under a nitrogen atmosphere by using conventional vacuum-line and inert-atmosphere techniques. $(TBA)_2$[Ir(CO)(CN)(mnt)] was prepared in an inert-atmosphere drybox because of the extreme hygroscopic nature of (TBA)CN and the sensitivity of $(TBA)_2$[Ir(CO)(CN)(mnt)] to H_2O and O_2, even in the solid state. In this case all solvents were refluxed over appropriate drying reagents and vacuum transferred prior to introduction into the drybox.

$MV(PF_6)_2$ was prepared by metathesis of the dichloride, $MVCl_2 \cdot 2H_2O$ (2.24 g, 0.871 mmol) with NH_4PF_6 in water. The resulting white precipitate was first dissolved in acetonitrile and filtered into stirred ether (to remove any $MVCl_2$ impurities) and then recrystallized from hot acetone/water and cooled at −20 °C for 3–5 h. This gave 2.70 g (70% yield) of $MV(PF_6)_2$ as white needles.

(TBA)PF_6 was prepared by metathesis of (TBA)Br (30 g, 0.093 mol) and NH_4PF_6 (16.5 g, 0.101 mol) in water. The resulting white precipitate was recrystallized from hot ethanol and then dried for 3 days under vacuum at 70–80 °C.

$(TBA)_2$[Ir(CO)(CN)(mnt)] (4). TBA[$Ir(CO)_2mnt$] (0.105 g, 0.166 mmol) and (TBA)CN (0.075 g, 0.279 mmol) were placed in a flask, and 2 mL of acetone was added. Vigorous gas evolution ensued, accompanied by a rapid color change from pale beige to yellow-brown. The solution was stirred for 10 min. Dropwise addition of 2 mL of diethyl ether followed by 6 mL of hexanes yielded a brown oil. This complex tends to oil due to presence of excess (TBA)CN. Repeated rapid precipitations of the oil from THF/diethyl ether resulted in the formation of a yellow-brown precipitate. The precipitate was collected by filtration and washed with diethyl ether to give 0.081 g (56%) of TBA_2[Ir(CO)(CN)(mnt)]. IR (cm^{-1}, KBr): 2189 (m, mnt ν_{CN}), 2082 (m, ν_{CN}), 1942 (s, ν_{CO}). UV/vis (nm (ϵ of PPN^+ salt[11]), CH_3CN): 438 (2800), 381 (4500), 338 (9200), 274 nm. Anal. Calcd for $IrC_{38}H_{72}N_5OS_2$: C, 52.38; H, 8.33; N, 8.04. Found: C, 52.36; H, 8.40; N, 7.98.

$MV[Ir(CO)_2(mnt)]_2$ (5). TBA[$Ir(CO)_2mnt$] (0.050 g, 0.079 mmol) and $MV(PF_6)_2$ (0.038 g, 0.080 mmol) were placed in a flask and dissolved in a minimum amount of acetonitrile (~5 mL). Initially a small amount of a bright orange precipitate formed, but it was dissolved by using sonication. The solution was allowed to sit overnight at −20 °C (freezer). The resultant bright orange cubic crystals were collected by filtration and washed once with cold 1:1 acetonitrile/ether to give 0.025 g (32%) of $MV[Ir(CO)_2(mnt)]_2$. IR (cm^{-1}, KBr): 2208 (m, ν_{CN}), 2041 (s, ν_{CO}), 1993 (m, ν_{CO}), 1969 (s, ν_{CO}), 1633 (m, MV^{2+} ν_{CC}), 1483 (m, mnt ν_{CC}). ^1H NMR (CD_3CN): δ 8.84 (s, b, 4 H) and 8.36 (s, b, 4 H) (MV^{2+} ring H), 4.40 (s, b, 6 H, CH_3 of MV^{2+}). Anal. Calcd for $Ir_2C_{24}H_{14}N_6O_4S_4$: C, 29.93; H, 1.47; N, 8.73. Found: C, 30.17; H, 1.38; N, 8.51. These crystals were used for the structure determination described below.

$[Ir(CO)(PPh_3)(mnt)]_2$ (6a). TBA[$Ir(CO)(PPh_3)(mnt)$] (0.025 g, 0.029 mmol) and $FcPF_6$ (0.013 g, 0.038 mmol) were placed in a flask, and 1–2 mL of acetonitrile was added. The red-brown solution was allowed to stand overnight, resulting in the formation of large red-black crystals. The crystals were collected by filtration and washed with CH_3CN and hexane to give 0.008 g (22%) of $[Ir(CO)(PPh_3)(mnt)]_2$. IR (cm^{-1}, CH_2Cl_2): 2227 (w, ν_{CN}), 2205 (m, ν_{CN}), 2033 (s, ν_{CO}). ^1H NMR (C_6D_6): δ 7.20 (q, 12 H, *o*-C_6H_5), 7.00 (t, 12 H, *m*-C_6H_5), 6.92 (d, 6 H, *p*-C_6H_5). ^{31}P NMR (C_6D_6): δ −16.39 (s, PPh_3).

$[Ir(CO)(P(p\text{-}tol)_3)(mnt)]_2$ (6b). This compound was prepared in a strictly analogous manner from TBA[$Ir(CO)(P(p\text{-}tol)_3)(mnt)$] (0.025 g, 0.028 mmol) and $FcPF_6$ (0.012 g, 0.036 mmol). Yield: 0.010 g (27%). IR (cm^{-1}, CH_2Cl_2): 2227 (w, ν_{CN}), 2204 (m, ν_{CN}), 2030 (s, ν_{CO}). ^1H NMR (C_6D_6): δ 7.28 (dd, 6 H, *o*-$C_6H_4CH_3$), 6.91 (d, 6 H, *m*-$C_6H_4CH_3$), 1.94 (s, 9 H, CH_3). ^{31}P NMR (C_6D_6): δ −17.99 (s, P(*p*-tolyl)$_3$). Anal. Calcd for $Ir_2C_{52}H_{42}N_4O_2P_2S_4$: C, 46.98; H, 3.18; N, 4.21. Found: C, 46.20; H, 3.08; N, 3.95. These crystals were used for the structure determination described below.

Table I. Selected Crystal Data and Data Collection and Structure Refinement Parameters[a]

	5	6b
formula	$Ir_2S_4O_4N_6C_{24}H_{14}$	$Ir_2S_4P_2O_2N_4C_{52}H_{42}$
fw	963.09	1329.56
space group	$C2/c$ (No. 15)	$P2_1/n$ (No. 14)
a, Å	14.754 (4)	14.874 (8)
b, Å	10.063 (3)	17.394 (5)
c, Å	19.985 (7)	19.99 (1)
β, deg	103.73 (3)	96.46 (5)
V, Å^3	2882	5140 (8)
Z	4	4
d_{calc}, g/cm^3	2.22	1.72
λ radiation (Mo Kα), Å	0.71069	0.71069
temp, °C	23	23
abs coeff [μ(Mo Kα)], cm^{-1}	101.06	57.51
transmissn coeff	0.78–1.37	0.72–1.21
$R(F_o)$	0.019	0.033
$R_w(F_o)$	0.026	0.040

Physical Measurements. Infrared spectra were obtained from KBr pellets or in methylene chloride (Baker Photorex) by using 0.1 mm CsBr plates on a Mattson Sirius 100 FTIR spectrometer. ^1H NMR spectra (300 MHz) were recorded on a General Electric QE-300 spectrometer. A Bruker WH-400 spectrometer was used to obtain ^{31}P (162.19 MHz) NMR spectra. Chemical shifts are reported in ppm downfield from external references (Me_4Si for ^1H and H_3PO_4 for ^{31}P) and calculated from internal solvent peaks (acetone-d_5 δ_H = 2.04, benzene-d_5 δ_H = 7.15, acetonitrile-d_2 δ_H = 1.93). UV–visible spectra were recorded on a Hewlett Packard HP-8451A diode-array spectrometer in 1-cm quartz cells at room temperature. Cyclic voltammetric experiments were carried out on a Princeton Applied Research 173 potentiostat and PAR 175 sweep generator and a Houston 200 XY recorder. A single-compartment, three-electrode cell containing a platinum (1.6 mm diameter) or glassy-carbon (3.2 mm diameter) disk working electrode, a platinum-gauze (0.25 cm^2) auxiliary electrode, and a saturated sodium calomel reference electrode (SSCE) were used for all measurements. Samples were dissolved in nitrogen-degassed acetonitrile with 0.1 M (TBA)PF_6 as supporting electrolyte. The metal-based oxidation was, in most cases, irreversible so E_{p_a} (anodic peak potentials) are reported except where noted.

Formation Constant Data. Extinction coefficients (ϵ_{AD}) for the CT band as well as ion-pair association constants (K_{AD}) were determined spectroscopically by using the method of Benesi and Hildebrand.[15] Since this procedure is relatively insensitive to the presence of higher order complexes,[16] measurements were taken under conditions where the MV^{2+} ion was present in at least 10-fold excess. The extent of ion-pair formation was determined by measuring the intensity of the CT band as a function of added MV^{2+} (large excess) for a fixed concentration of iridium complex. For a single concentration of iridium complex, a 10–200-fold excess of methyl viologen was added. This was repeated over a 10-fold range of Ir complex. The temperature of the cuvette was maintained at 23 ± 2 °C.

Samples for the determination of K_{AD} and ϵ_{AD} of the CT complexes were prepared in the following manner. A known amount of Ir complex was weighed into a 10-mL volumetric flask and diluted to the mark with freshly distilled acetonitrile. Then, 5 mL of this solution was transferred to a quartz curvette and the UV/vis spectrum taken. This spectrum was stored on disk and later used for reference. To this sample of known Ir concentration was added various, accurately weighed amounts of MV$(PF_6)_2$ as a solid; the solutions were then shaken well and the visible spectra were recorded. For each Ir concentration, a minimum of six MV^{2+} concentrations were used.

Structure Determinations. Crystal Structure Determination of $MV[Ir(CO)_2(mnt)]_2$ (5). A crystal suitable for X-ray diffraction study was grown from cold acetonitrile. Crystal data and data collection parameters are summarized in Table I. Heavy-atom methods were employed to locate the iridium and two sulfur atoms. Subsequent cycles of least-squares refinements and difference Fourier maps located the remaining

(12) Davison, A.; Holm, R. H. *Inorg. Synth.* **1967**, *10*, 8.
(13) (a) Duggan, D. M.; Hendrickson, D. N. *Inorg. Chem.* **1975**, *14*, 955. (b) Hendrickson, D. N.; Sohn, Y. S.; Gray, H. B. *Inorg. Chem.* **1971**, *10*, 1559.
(14) Cleare, M. J.; Griffith, W. P. *J. Chem. Soc. A* **1970**, 2788.
(15) Benesi, H. A.; Hildebrand, J. H. *J. Am. Chem. Soc.* **1949**, *71*, 2703.
(16) (a) Foster, R. *Organic Charge-Transfer Complexes*; Academic Press: New York, 1969. (b) Slifkin, M. A. *Charge Transfer Interactions in Biomolecules*; Academic Press: New York, 1971.

Table II. Refined Positional and Isotropic Thermal Parameters and Their Estimated Standard Deviations for $MV[Ir(CO)_2(mnt)]_2$[a]

atom	x	y	z	B(eq), Å²
Ir	0.20023 (2)	0.15024 (2)	0.16434 (1)	3.01 (1)
S1	0.1350 (1)	0.3564 (1)	0.17133 (8)	3.76 (6)
S2	0.0787 (1)	0.1027 (2)	0.07126 (8)	3.69 (6)
O1	0.2941 (3)	−0.1095 (5)	0.1519 (3)	5.4 (2)
O2	0.3509 (3)	0.2102 (5)	0.2895 (3)	6.1 (2)
N1	−0.0601 (4)	0.5685 (5)	0.0836 (3)	5.6 (3)
N2	−0.1380 (4)	0.2438 (6)	−0.0341 (3)	5.8 (3)
N3	0.8295 (3)	0.0273 (4)	0.5959 (2)	3.3 (2)
C1	0.0369 (4)	0.3531 (5)	0.1023 (3)	3.2 (2)
C2	0.0135 (4)	0.2482 (5)	0.0616 (3)	3.0 (2)
C3	−0.0175 (4)	0.4732 (6)	0.0917 (3)	3.7 (3)
C4	−0.0698 (4)	0.2476 (6)	0.0070 (3)	3.9 (2)
C5	0.2560 (4)	−0.0119 (6)	0.1561 (3)	3.9 (3)
C6	0.2934 (4)	0.1881 (6)	0.2415 (3)	4.2 (3)
C7	0.9647 (4)	0.0201 (5)	0.7159 (3)	3.1 (2)
C8	0.9506 (4)	0.1327 (5)	0.6753 (3)	3.5 (2)
C9	0.8822 (4)	0.1330 (5)	0.6155 (3)	3.6 (2)
C10	0.8423 (4)	−0.0836 (5)	0.6334 (3)	3.8 (3)
C11	0.9093 (4)	−0.0915 (6)	0.6925 (3)	3.7 (2)
C12	0.7526 (5)	0.0352 (7)	0.533 (3)	4.6 (3)

[a] Values for anisotropically refined atoms are given in the form of the isotropic equivalent thermal parameter defined as $(4/3)[a^2B(1,1) + b^2B(2,2) + c^2B(3,3) + ab(\cos\gamma)B(1,2) + ac(\cos\beta)B(1,3) + bc(\cos\alpha)B(2,3)]$.

non-hydrogen atoms. The methyl viologen cation possesses crystallographic C_2 symmetry. In the last refinement all non-hydrogen atoms were described with anisotropic thermal parameters. Hydrogen atoms were placed at calculated positions around the methylpyridinium rings. Table II contains the final refined positional and isotropic thermal parameters for the structure. The supplementary material contains the final anisotropic thermal parameters, the calculated hydrogen positional parameters, a complete tabulation of bond distances and angles, and a listing of observed and calculated structure factor amplitudes for the structure. See paragraph regarding supplementary material at end of paper.

Crystal Structure Determination of $[Ir(CO)(P(p\text{-tol})_3)(mnt)]_2$ (6b). A crystal of **6b** was grown from room-temperature acetonitrile solution of $[Ir(CO)(P(p\text{-tol})_3)(mnt)]^-$ and Fc^+. Crystal data and data collection parameters are summarized in Table I. Heavy-atom methods were employed to locate the two iridium, two phosphorus, and four sulfur atoms, and subsequent cycles of least-squares refinements and difference Fourier maps located the remaining non-hydrogen atoms. In the last refinement all non-hydrogen atoms were described with anisotropic thermal parameters. Hydrogen atoms were placed at calculated positions around the tolyl rings. Table III contains the final refined positional and isotropic thermal parameters for the structure. Supplementary material contains the final anisotropic thermal parameters, the calculated hydrogen positional parameters, a complete tabulation of bond distances and angles, and a listing of observed and calculated structure factor amplitudes for the structure. See paragraph regarding supplementary material at end of paper.

Results and Discussion

In a previous study of $IrLL'(mnt)^{n-}$ complexes, their luminescence was studied.[11] It was found that λ_{em} varied as a function of ligand donor ability and that the emitting state was a metal-to-ligand ($d-\pi^*_{mnt}$) charge transfer. Since ligand donor ability influences the position of the HOMO in these complexes, a similar correlation should exist between the ligand donor ability and the reducing power of these complexes as shown by their oxidation potentials.

Electrochemistry. The electrochemistry of the $IrLL'(mnt)^{n-}$ complexes in acetonitrile solution with 0.1–0.2 M $(TBA)PF_6$ as supporting electrolyte exhibits two redox couples—an irreversible, or at least quasi-reversible, one-electron oxidation between 0.16 and 0.50 V vs SSCE and a reversible one-electron reduction in the range −1.8 to −2.4 V vs SSCE. Oxidation potentials for these complexes are given in Table IV. The irreversibility of the electrochemistry indicates either that the back electron transfer is slow or that there is a chemical reaction following the electron transfer. Although the oxidations are irreversible, the relative ordering of these potentials suggests that the reducing ability of these complexes does vary with the ligand donor ability—a result that led to different observations for these complexes ranging from thermal electron transfer to optical charge transfer.

Acetonitrile solutions of $MV(PF_6)_2$ exhibit two reversible one-electron reductions at −0.45 and −0.88 V vs SSCE. These

Table III. Refined Positional and Isotropic Thermal Parameters and Their Estimated Standard Deviations for $[Ir(CO)(P(p\text{-tol})_3)(mnt)]_2$[a]

atom	x	y	z	B(eq), Å²
Ir1	0.43073 (2)	0.20491 (2)	0.13600 (2)	2.66 (2)
Ir2	0.24876 (2)	0.20686 (2)	0.10579 (2)	2.75 (2)
S1	0.4499 (2)	0.1248 (1)	0.2305 (1)	4.0 (1)
S2	0.3314 (2)	0.2796 (1)	0.1922 (1)	3.0 (1)
S3	0.2226 (2)	0.1174 (2)	0.0182 (1)	4.8 (1)
S4	0.3504 (2)	0.2706 (1)	0.0432 (1)	3.0 (1)
P1	0.1201 (2)	0.2862 (1)	0.0831 (1)	2.9 (1)
P2	0.5606 (2)	0.2792 (1)	0.1667 (1)	3.1 (1)
O1	0.5073 (6)	0.0915 (5)	0.0455 (4)	6.6 (5)
O2	0.1798 (5)	0.1062 (5)	0.2082 (5)	6.8 (5)
N1	0.3802 (8)	0.0999 (6)	0.3990 (5)	6.8 (6)
N2	0.2469 (9)	0.2937 (8)	0.3586 (6)	8.9 (7)
N3	0.4604 (9)	0.2519 (8)	−0.1117 (6)	8.7 (7)
N4	0.298 (1)	0.0683 (8)	−0.1449 (6)	11 (1)
C1	0.3841 (6)	0.1671 (6)	0.2840 (5)	3.8 (5)
C2	0.3319 (6)	0.2334 (5)	0.2697 (5)	3.2 (4)
C3	0.3823 (7)	0.1297 (7)	0.3478 (5)	4.6 (5)
C4	0.2862 (8)	0.2669 (7)	0.3195 (6)	4.96 (6)
C5	0.2949 (8)	0.1483 (6)	−0.0364 (6)	4.9 (6)
C6	0.3496 (7)	0.2115 (6)	−0.0281 (5)	3.9 (5)
C7	0.4086 (8)	0.2325 (8)	−0.0744 (6)	5.4 (6)
C8	0.299 (1)	0.1037 (7)	−0.0961 (7)	6.9 (7)
C9	0.4797 (6)	0.1330 (6)	0.0802 (5)	3.6 (5)
C10	0.2026 (7)	0.1433 (6)	0.1695 (5)	3.4 (5)
C11	0.0112 (6)	0.2387 (6)	0.0628 (5)	3.2 (4)
C12	−0.0607 (7)	0.2792 (6)	0.0286 (6)	4.5 (5)
C13	−0.1438 (7)	0.2467 (8)	0.0174 (6)	5.4 (6)
C14	−0.1588 (7)	0.1723 (7)	0.0395 (6)	4.5 (6)
C15	−0.0894 (7)	0.1329 (6)	0.0725 (6)	4.8 (6)
C16	−0.0046 (7)	0.1657 (6)	0.0829 (6)	4.3 (5)
C17	−0.2528 (7)	0.1377 (8)	0.0247 (6)	6.4 (7)
C21	0.1278 (6)	0.3532 (5)	0.0152 (5)	3.1 (4)
C22	0.1511 (7)	0.3265 (5)	−0.0461 (5)	3.7 (5)
C23	0.1527 (7)	0.3757 (6)	−0.1010 (5)	4.3 (5)
C24	0.1309 (7)	0.4512 (6)	−0.0963 (5)	3.9 (5)
C25	0.1093 (7)	0.4792 (5)	−0.0356 (6)	4.3 (5)
C26	0.1069 (6)	0.4307 (5)	0.0198 (5)	3.7 (5)
C27	0.1297 (8)	0.5049 (6)	−0.1553 (6)	5.5 (6)
C31	0.1070 (6)	0.3421 (5)	0.1585 (5)	3.2 (4)
C32	0.0443 (7)	0.3205 (6)	0.2010 (5)	4.6 (5)
C33	0.428 (9)	0.3560 (7)	0.2619 (6)	5.4 (6)
C34	0.1036 (8)	0.4134 (6)	0.2842 (5)	4.6 (6)
C35	0.1621 (7)	0.4361 (6)	0.2389 (6)	4.3 (5)
C36	0.1161 (6)	0.4018 (5)	0.1780 (5)	3.6 (5)
C37	0.102 (1)	0.4474 (7)	0.3517 (7)	7.6 (8)
C41	0.6656 (6)	0.2281 (5)	0.1947 (5)	3.3 (5)
C42	0.6714 (6)	0.1500 (5)	0.1924 (5)	3.6 (5)
C43	0.7533 (7)	0.1136 (6)	0.2125 (6)	4.6 (5)
C44	0.8279 (7)	0.1543 (7)	0.2379 (5)	4.6 (6)
C45	0.8205 (7)	0.2330 (7)	0.2402 (6)	5.3 (6)
C46	0.7407 (7)	0.2698 (6)	0.2183 (6)	5.1 (6)
C47	0.9151 (8)	0.1141 (8)	0.2604 (7)	7.0 (7)
C51	0.52388 (6)	0.3368 (5)	0.2391 (5)	3.2 (4)
C52	0.4867 (7)	0.4025 (5)	0.2299 (5)	3.9 (5)
C53	0.4564 (7)	0.4391 (6)	0.2861 (6)	4.4 (5)
C54	0.4758 (7)	0.4107 (6)	0.3491 (6)	4.2 (5)
C55	0.5295 (8)	0.3451 (7)	0.3586 (6)	5.2 (6)
C56	0.5603 (7)	0.3090 (6)	0.3039 (5)	4.3 (5)
C57	0.438 (1)	0.4474 (8)	0.4079 (7)	7.8 (8)
C61	0.5911 (6)	0.3456 (6)	0.1028 (5)	3.9 (5)
C62	0.6218 (8)	0.4194 (6)	0.1166 (6)	5.4 (6)
C63	0.6407 (9)	0.4677 (7)	0.0642 (8)	6.6 (7)
C64	0.6322 (8)	0.4433 (8)	−0.0010 (7)	6.0 (7)
C65	0.6027 (9)	0.3698 (8)	−0.0153 (6)	6.2 (7)
C66	0.5825 (7)	0.3211 (6)	0.0363 (6)	4.5 (5)
C67	0.654 (1)	0.496 (1)	−0.0573 (8)	10 (1)

[a] Anisotropically refined atoms are given in the form of the isotropic equivalent thermal parameter defined as $(4/3)[a^2B(1,1) + b^2B(2,2) + c^2B(3,3) + ab(\cos\gamma)B(1,2) + ac(\cos\beta)B(1,3) + bc(\cos\alpha)B(2,3)]$.

Table IV. Electrochemical Potentials for TBA[Ir(L)(L')(mnt)] Complexes in Acetonitrile with 0.13 M $(TBA)PF_6$ Supporting Electrolyte[a]

complex	$E_{1/2}$(Ir(I/0)), V	E_{p_a}(Ir(I/II)), V	$E_{1/2}$(Ir(II/I)), V
L = L' = CO	-2.00	0.51	0.41
L = L' = $P(OPh_3)$	-2.21	0.41	
L = CO, L' = PPh_3	-2.29	0.33	
L = CO, L' = CN	-2.41	0.16	

[a] Electrodes: glassy carbon working; platinum gauze, auxiliary; SSCE, reference. Potentials reported vs SSCE.

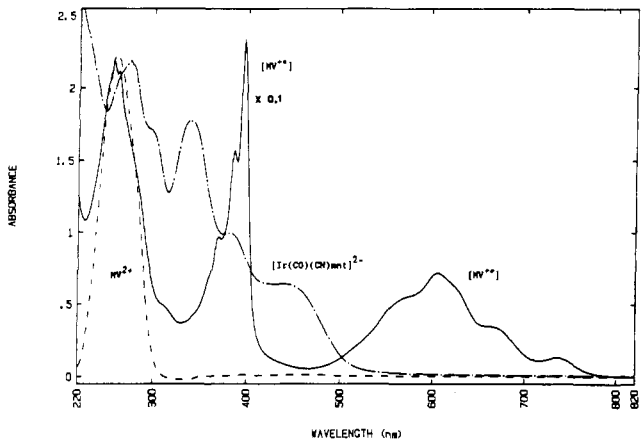

Figure 2. UV/visible spectra in acetonitrile solution: (a) $(TBA)_2$[Ir(CO)(CN)(mnt)] (-·-); (b) $MV(PF_6)_2$ (---); (c) $(TBA)_2$[Ir(CO)(CN)(mnt)] + $MV(PF_6)_2$ (—). The scale in part c is one-tenth that in parts a and b.

results agree well with previously reported values[17] and are assigned to the reductions

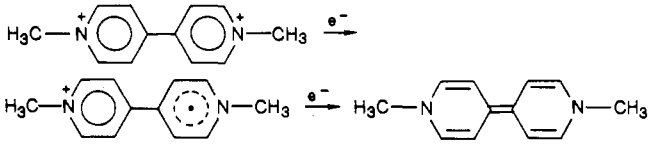

Thermal Electron Transfer. When $Ir(CO)(CN)(mnt)^{2-}$, the most reducing of the four complexes, is added to a solution of MV^{2+} under nitrogen, the spectrum shown in Figure 2 results. One observes the immediate formation of $MV^{\bullet+}$ as evidenced by the presence of a structured absorbance with a maximum at 606 nm (ϵ = 13 900 cm^{-1} M^{-1})[18] giving the solution an intense blue color. This behavior is indicative of facile thermal one electron transfer. Calculation of $MV^{\bullet+}$ concentration from the absorbance at 606 and 732 nm shows essentially quantitative conversion of Ir(I) to Ir(II). The nature of the Ir product has not been established, but it is no doubt related to the Ir(II) dimer discussed below. Evidence to support this comes from IR data for the yellow oil obtained from the reaction solution, which shows two ν_{CN} bands for the mnt ligand at 2219 and 2197 cm^{-1} and a single ν_{CN} band for CN^- at 2124 cm^{-1}. There is no ν_{CO} band, suggesting that the CO ligand is lost during oxidation of the parent Ir(I) complex, and ^1H NMR data on this product in DMSO-d_6 indicate that this complex is paramagnetic.

While thermal electron transfer is clearly seen in solutions of **4** and MV^{2+}, the thermodynamics of this system cannot be calculated since the oxidation of **4** is irreversible and its $E_{1/2}$ value for the Ir(II/I) couple is not known.

Optical Electron Transfer. The least reducing Ir(I) complex, $Ir(CO)_2(mnt)^-$, forms solutions with MV^{2+} in acetonitrile that show a broad charge-transfer (CT) band seen as a shoulder in Figure 3. This CT shoulder, at 470 nm (±2 nm), on the low-

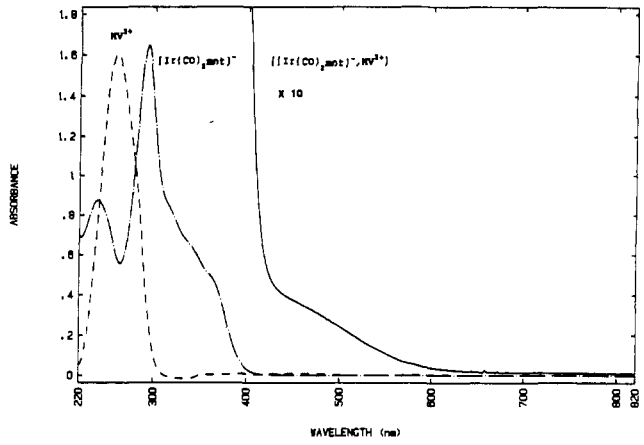

Figure 3. UV/visible spectra in acetonitrile solution: (a) TBA[Ir(CO)$_2$(mnt)] (-·-); (b) $MV(PF_6)_2$ (---); (c) TBA[Ir(CO)$_2$(mnt)] + $MV(PF_6)_2$ (—). The scale in part c is 10 times that in prts a and b.

energy side of a $Ir(CO)_2(mnt)^-$ transition is observed under all sets of conditions studied: rigorously N_2 degassed or open to the air—in the dark, under exposure to room light, or even under direct photolysis. The extinction coefficient for the CT band as well as the ion-pair association constant was determined spectroscopically in 0.1 M $TBA(PF_6)_2$ solutions by using the Benesi–Hildebrand (B-H) method[15,16] and the equation described by Ketelaar[19] and Nash[20] to compensate for any small absorption of the iridium complex (eq 3). The value of the association constant (K_{AD}) was obtained from the slope of the plot of $1/(\epsilon_{obs} - \epsilon_{Ir(470nm)})$ vs $1/[MV^{2+}]$ by using the extrapolated value of the extinction coefficient (ϵ_{AD}) at the intercept and assuming the formation of 1:1 complexes. The values obtained in this manner are ϵ_{AD} = 270 ± 20 cm^{-1} M^{-1} and K_{AD} = 10 ± 5 M^{-1}

$$\frac{1}{\epsilon_{obs} - \epsilon_D} = \frac{1}{K_{AD}(\epsilon_{AD} - \epsilon_D)} \frac{1}{[A]_0} + \frac{1}{\epsilon_{AD} - \epsilon_D} \qquad (3)$$

where ϵ_{obs} = Abs/$[D]_0 l$, Abs = observed absorbance, $[D]_0$ = initial concentration of the donor complex (the Ir(I) anion), l = cell path length (1 cm), ϵ_D = extinction coefficient of the donor at the wavelength under study (ϵ of the iridium complex anion), K_{AD} = association constant for the acceptor–donor complex, ϵ_{AD} = extinction coefficient for the donor–acceptor complex at the wavelength under study, $[A]_0$ = initial concentration of the acceptor complex (MV^{2+}).

To avoid complications arising from higher order complexes, all measurements were carried out with the methyl viologen in excess. For these systems, higher order complexes are expected based on charge attraction, and in fact, the crystal structure data bear this out. The magnitude of K_{AD} is rather small, indicative of a weakly bound charge-transfer complex. The magnitude of ϵ_{AD} is also small. K_{AD} and ϵ_{AD} were determined over a range of Ir(I) and MV^{2+} concentrations. Under all circumstances the observed values of K_{AD} and ϵ_{AD} were relatively constant, although at lower concentrations of Ir(I), 1 mM, the magnitudes of K_{AD} and ϵ_{AD} were larger than at higher concentrations, 5 mM—K_{AD} = 15 vs 7 M^{-1}, and ϵ_{AD} = 280 vs 240 cm^{-1}. This may indicate that above a certain concentration of Ir(I) anion, even in the presence of a large excess of MV^{2+}, termolecular complexes such as $MV[Ir(CO)_2(mnt)]_2$ are formed.

Attempts to determine ϵ_{AD} using more accurate 1:1 ratios[7c,16] of $Ir(L)_2(mnt)^-$ of MV^{2+} failed as plots were not linear at low concentrations, indicating the ion-pair formation was not complete, and at high concentrations a crystalline precipitate was formed that was later identified as the charge-transfer complex $MV[Ir(CO)_2(mnt)]_2$.

In addition to its CT band in the visible spectrum, this complex exhibits differences in the ^1H NMR and FTIR spectra compared

(17) Dressick, W. Ph.D. Dissertation, The University of North Carolina, Chapel Hill, NC, 1981.
(18) (a) Watanabe, T.; Honda, K. *J. Phys. Chem.* **1982**, *86*, 2617. (b) Tsukahara, K.; Wilkins, R. G. *J. Am. Chem. Soc.* **1985**, *107*, 2632.
(19) Ketelaar, J. A. A.; van de Stolpe, C.; Goudsmit, A.; Dzcubas, W. *Recl Trav. Chim. Pays-Bas Belg.* **1952**, *71*, 1104.
(20) Nash, C. P. *J. Phys. Chem.* **1960**, *64*, 950.

Table V. Selected Bond Distances (Å) for $MV[Ir(CO)_2(mnt)]_2$[a]

Ir–C6	1.846 (6)	N3–C10	1.333 (7)
Ir–C5	1.852 (7)	N3–C12	1.478 (7)
Ir–S1	2.305 (2)	C1–C2	1.327 (7)
Ir–S2	2.306 (2)	C1–C3	1.439 (8)
S1–C1	1.746 (6)	C2–C4	1.437 (8)
S2–C2	1.737 (6)	C7–C8	1.380 (7)
O1–C5	1.145 (7)	C7–C11	1.403 (8)
O2–C6	1.142 (7)	C7–C7	1.51 (7)
N1–C3	1.137 (7)	C8–C9	1.368 (8)
N2–C4	1.139 (7)	C10–C11	1.350 (8)
N3–C9	1.322 (6)		

[a] Estimated standard deviations in the least significant figure are given in parentheses.

Table VI. Selected Bond Angles (deg) for $MV[Ir(CO)_2(mnt)]_2$[a]

C6–Ir–C5	89.8 (3)	C1–C2–C4	121.4 (5)
C6–Ir–S1	90.2 (2)	C1–C2–S2	123.0 (4)
C6–Ir–S2	177.3 (2)	C4–C2–S2	115.6 (4)
C5–Ir–S1	177.3 (2)	N1–C3–C1	179.6 (7)
C5–Ir–S2	91.3 (2)	N2–C4–C2	176.5 (7)
S1–Ir–S2	88.84 (6)	O1–C5–Ir	177.1 (5)
C1–S1–Ir	102.4 (2)	O2–C6–Ir	179.3 (5)
C2–S2–Ir	102.6 (2)	C8–C7–C11	117.9 (5)
C9–N3–C10	120.8 (5)	C8–C7–C7	120.5 (3)
C9–N3–C12	119.2 (5)	C11–C7–C7	121.6 (4)
C10–N3–C12	120.0 (5)	C9–C8–C7	119.5 (5)
C2–C1–C3	121.5 (5)	N3–C9–C8	121.2 (5)
C2–C1–S1	123.1 (4)	N3–C10–C11	121.2 (5)
C3–C1–S1	115.4 (4)	C10–C11–C7	119.4 (5)

[a] Estimated standard deviations in the least significant figure are given in parentheses.

with the spectra of MV^{2+} and $[Ir(CO)_2(mnt)]^-$ individually. ^1H NMR spectra of the isolated CT complex show three broad singlets at δ 8.84, 8.36, and 4.40 for MV^{2+}, while $MV(PF_6)_2$ exhibits two doublets and a singlet, respectively, at those chemical shifts. While the broadening observed for the former may be suggestive of exchange, its basis has not been unambiguously established. The FTIR spectrum of isolated $MV[Ir(CO)_2(mnt)]_2$ in the solid state exhibits an additional ν_{CO} band at 1993 cm^{-1} not present in the solution spectrum of the CT complex or in either the solid or the solution spectrum of $TBA[Ir(CO)_2(mnt)]$ starting material. However, since this stretch is only seen in the solid state, it may be due to a crystal packing effect.

Crystal Structure Determination for $MV[Ir(CO)_2(mnt)]_2$. The molecular structures of MV^{2+} and $[Ir(CO)_2(mnt)]^-$ in $MV[Ir(CO)_2(mnt)]_2$ as determined by crystal structure analysis are shown in Figure 4. Selected bond distances and angles for $MV[Ir(CO)_2(mnt)]_2$ are tabulated in Tables V and VI while complete listings of these parameters are provided in the supplementary material. The local geometry about the Ir(I) atom is square planar (Figure 4a). The Ir–S bond distances average 2.305 (1) Å, which is significantly shorter than previously reported Ir–S bond distances, 2.332 (5)–2.396 (9) Å,[21,22] for octahedrally coordinated Ir(III) complexes. The shorter bond length observed here is consistent with tighter coordination of the mnt ligand to remove excess electron density from the more electron-rich Ir(I) atom and is in good agreement with those of square-planar Rh(I) mnt complexes.[23] Other mnt bond lengths agree with those reported previously for metal–mnt complexes.[21,23] The Ir–C(carbonyl) bond distances average 1.849 (3) Å and are in agreement with previously reported Ir–CO bond distances.[21-24]

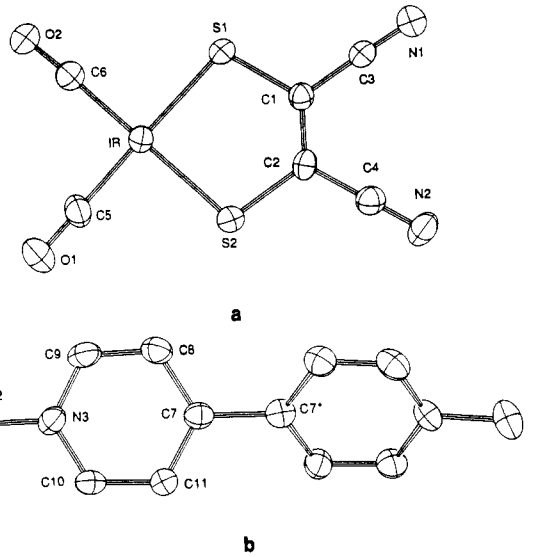

Figure 4. Molecular structures and atom numbering (ORTEP diagram, 35% thermal ellipsoids): (a) $[Ir(CO)_2(mnt)]^-$; (b) MV^{2+}. Hydrogen atoms have been omitted.

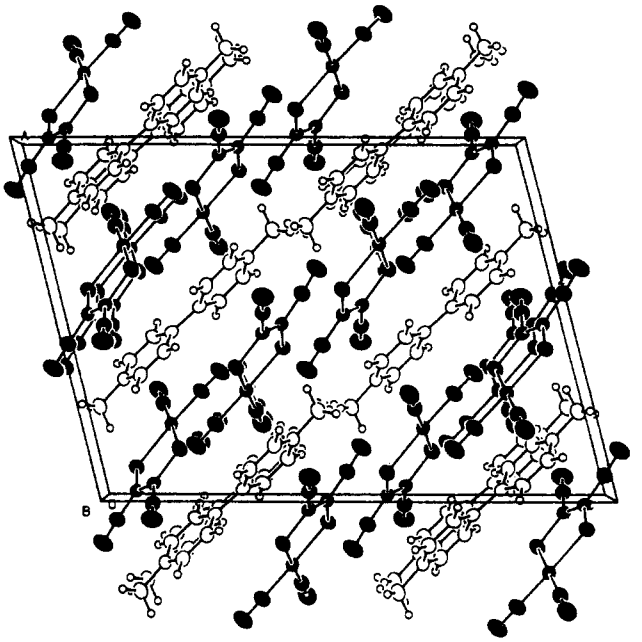

Figure 5. Packing diagram of **5** with thermal ellipsoids drawn at the 50% level. Closed ellipsoids represent the atoms of the $[Ir(CO)_2(mnt)]^-$ anions while the open circles represent the atoms of the MV^{2+} cations.

The methyl viologen bond distrances also agree with those of previously reported structures.[25,26] The interesting feature here is twisting about the C–C bond between the two planar methylpyridinium rings (Figure 4b). The dihedral angle between the planes of the two rings is 37.79°. This type of distortion has

(21) (a) Khare, G. P.; Eisenberg, R. *Inorg. Chem.* **1972**, *11*, 1385. (b) Bradley, P.; Johnson, C. E.; Eisenberg, R. *J. Chem. Soc., Chem. Commun.* **1988**, 255. (c) Bradley, P. Doctoral Dissertation, University of Rochester, Rochester, NY, 1988.

(22) (a) Edelman, F.; Roesky, H. W.; Spang, C.; Noltemeyer, M.; Sheldenk, G. M.; *Angew. Chem.* **1986**, *98*, 908. (b) Claver, C.; Fis, J.; Kalck, P.; Jaud, J. *Inorg. Chem.* **1987**, *26*, 3479.

(23) (a) VanDerveer, D. G.; Eisenberg, R. *J. Am. Chem. Soc.* **1974**, *96*, 4994. (b) Cheng, C.-H.; Eisenberg, R. *Inorg. Chem.* **1979**, *18*, 2438. (c) Cheng, C.-H.; Eisenberg, R. *Inorg. Chem.* **1979**, *18*, 1418.

(24) (a) Behrens, U.; Dahlenburg, L. *J. Organomet. Chem.* **1976**, *116*, 103. (b) Brown, L. D.; Ibers, J. A.; Siedle, A. R. *Inorg. Chem.* **1978**, *17*, 3026. (c) Sutherland, B. R.; Cowie, M. *Organometallics* **1985**, *4*, 1637. (d) Wang, H.-H.; Pignolet, L. H.; Reedy, P. E.; Olmstead, M. M.; Balch, A. L. *Inorg. Chem.* **1987**, *26*, 377. (e) Rasmussen, P. G.; Anderson, J. E.; Bailey, O. H.; Tamres, M.; Bayn, J. C. *J. Am. Chem. Soc.* **1985**, *107*, 279.

(25) (a) Russell, J. H.; Wallwork, S. C. *Acta Crystallogr.* **1969**, *B25*, 1691. (b) Russell, J. H.; Wallwork, S. C. *Acta Crystallogr.* **1972**, *B28*, 1527. (c) Murray-Rust, P. *Acta Crystallogr.* **1975**, *B31*, 1771. (d) Mahmoud, M. M.; Wallwork, S. C. *Acta Crystallogr.* **1976**, *B32*, 440. (e) Ashwell, G. J.; Wallwork, S. C. *Acta Crystallogr.* **1979**, *B35*, 1648. (f) Mahmoud, M. M.; Wallwork, S. C. *Acta Crystallogr.* **1981**, *B37*, 398.

(26) (a) Prout, C. K.; Murray-Rust, P. *J. Chem. Soc. A* **1969**, 1520. (b) Nakamura, K.; Kai, Y.; Yasuoka, N.; Kasai, N. *Bull. Chem. Soc. Jpn.* **1981**, *54*, 3300.

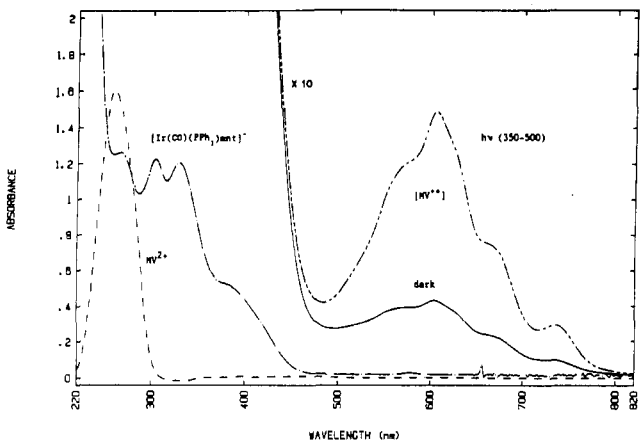

Figure 6. UV/visible spectra in acetonitrile solution: (a) TBA[Ir(CO)(PPh$_3$)(mnt)] (---); (b) MV(PF$_6$)$_2$ (---); (c) TBA[Ir(CO)(PPh$_3$)(mnt)] + MV(PF$_6$)$_2$ (—) in the dark; (d) solution from part c after photolysis with 350–500-nm light for 30 min (----). The scale in parts c and d is 10 times that of parts a and b.

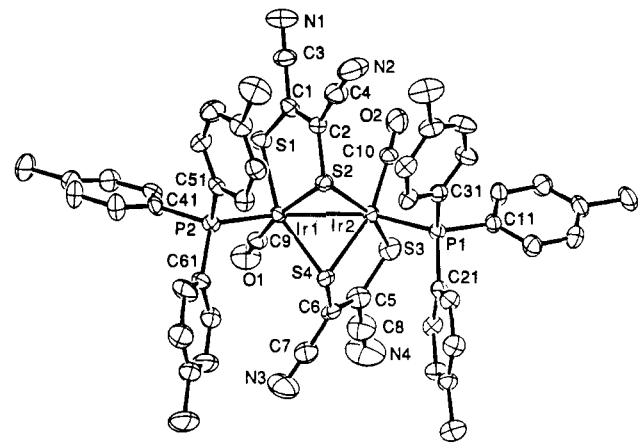

Figure 7. ORTEP drawing of [Ir(CO)(P(*p*-tol)$_3$)(mnt)]$_2$ showing the molecular structure and the numbering scheme used. Thermal ellipsoids were drawn at the 35% level. Tolyl hydrogen atoms have been omitted for clarity.

been previously reported for [MV][PdCl$_4$][26a] and [MV][TCPD][26b] (TCPD = 1,1,3,3-tetracyanopropanediide) with dihedral angles of 50 and 19.6 (2)°, respectively, and may be due to crystal packing effects. The majority of crystal structures of charge-transfer complexes containing MV^{2+} and both organic and inorganic anions show planar methyl viologen molecules.

Figure 5 shows the packing diagram for MV[Ir(CO)$_2$(mnt)]$_2$. The crystal consists of alternating infinite sheets of Ir(I) anions and MV^{2+} cations. The planar Ir(I) anion forms a dihedral angle of 9.2° with the plane of one ring of each nearest neighbor MV^{2+}, which is separated from it by distances in the range 3.2–3.6 Å.

Photoassisted Electron Transfer. Acetonitrile solutions of Ir(CO)(PPh$_3$)(mnt)$^-$ and methyl viologen prepared in the dark give rise to a structured absorbance at 606 nm characteristic of MV$^{\bullet+}$ as shown in Figure 6. The intensity of the MV$^{\bullet+}$ absorbance indicates that <5% of the initial Ir(I) complex has been oxidized. A sample left in the dark shows a gradual increase in the intensity of this absorbance over 24 h until it stabilizes at a final MV$^{\bullet+}$ concentration corresponding to 15% of the Ir(I) complex being oxidized. Further, if a sample (prepared from the same stock solution and placed in a second cell) is photolyzed with 350–500-nm light, the MV$^{\bullet+}$ concentration increases rapidly until 15% of the starting Ir(I) complex is oxidized and stabilizes within 30 min. Prolonged photolysis (4 h) does not increase the amount of MV$^{\bullet+}$ present in solution, nor does the absorbance at 606 nm decrease when the photolysis solution is placed in the dark provided the solution is kept under nitrogen (exposure to oxygen causes rapid oxidation of MV$^{\bullet+}$ back to MV^{2+}).

While these results indicate that thermal electron transfer is accessible in this system and that electron transfer can be promoted photochemically, they also show that the redox reaction does not go to completion. The system does not, however, attain chemical equilibrium since the Ir(II) product slowly reacts to form a more stable species via dimerization.

Oxidation of Ir(CO)(PR$_3$)(mnt)$^-$ and Crystal Structure Determination. In order to determine the nature of this Ir(II) product, the oxidation of Ir(CO)(PR$_3$)(mnt)$^-$ was performed chemically by using the known one-electron oxidant, the ferrocenium ion, Fc$^+$.[27] For R = Ph and *p*-tolyl, dimers of formula [Ir(CO)(PR$_3$)(mnt)]$_2$ were readily obtained by using Fc$^+$ at room temperature in nitrogen-degassed acetonitrile solutions; crystals of the R = *p*-tolyl derivative suitable for X-ray study were grown directly from the reaction solution. The molecular structure of [Ir(CO)(P(*p*-tol)$_3$)(mnt)]$_2$ is shown in Figure 7, and the packing diagram is shown in Figure S1 (supplementary material). In the structure, each mnt ligand is chelated to one Ir atom with one sulfur atom of each mnt bridging the two Ir atoms, which are connected by an Ir–Ir single bond of length 2.706 (2) Å. This Ir–Ir bond length is comparable to that found in a number of ligand-bridged Ir dimers (2.638–2.785 Å)[28] and to Ir–Ir distances of 2.714 Å found in the pure iridium metal.[29]

Table VII. Selected Bond Distances (Å) for [Ir(CO)(P(*p*-tol)$_3$)(mnt)]$_2$[a]

Ir1–C9	1.88 (1)	P1–C11	1.82 (1)
Ir1–S1	2.340 (3)	P2–C61	1.82 (1)
Ir1–S2	2.346 (3)	P2–C51	1.82 (1)
Ir1–P2	2.348 (3)	P2–C41	1.829 (9)
Ir1–S4	2.382 (3)	O1–C9	1.11 (1)
Ir1–Ir2	2.706 (2)	O2–C10	1.09 (1)
Ir2–C10	1.87 (1)	N1–C3	1.15 (1)
Ir2–S3	2.342 (3)	N2–C4	1.13 (1)
Ir2–S4	2.347 (3)	N3–C7	1.18 (1)
Ir2–P1	2.362 (3)	N4–C8	1.15 (1)
Ir2–S2	2.370 (3)	C1–C2	1.40 (1)
S1–C1	1.70 (1)	C1–C3	1.44 (1)
S2–C2	1.74 (1)	C2–C4	1.40 (1)
S3–C5	1.70 (1)	C5–C6	1.37 (1)
S4–C6	1.76 (1)	C5–C8	1.43 (2)
P1–C21	1.80 (1)	C6–C7	1.39 (2)
P1–C31	1.82 (1)		

[a] Estimated standard deviations in the least significant figure are given in parentheses.

The coordination geometry about each Ir is essentially distorted square pyramidal if the stereochemical influence of the Ir–Ir bond is ignored. The P(*p*-tol)$_3$ ligand occupies the apical position at each Ir while the basal ligands consist of a carbonyl, a bidentate mnt, and a bridging S from the other mnt ligand of the dimer. The two phosphorus and two iridium atoms of the dimer lie in a plane with P–Ir–Ir bond angles of 145° and the P(*p*-tol)$_3$ groups on the same side of the Ir–Ir bond. The dimer is symmetrical and has a C_2 axis midway between the two iridium atoms in the P–Ir–Ir–P plane.

Selected bond distances and angles for [Ir(CO)(P(*p*-tol)$_3$)(mnt)]$_2$ are tabulated in Tables VII and VIII while complete listings of these parameters are provided in the supplementary material. The Ir–S(chelate) distance is 2.344 (3) Å. By contrast, the Ir–S(bridging) distances (Ir1–S4 and Ir2–S2) are statistically inequivalent, 2.382 (3) and 2.370 (3) Å, respectively, and are

(27) Fc$^+$ was chosen as the chemical oxidant because (a) its reduction potential is sufficiently positive for reaction to occur—$E_{1/2}$(Fc$^+$/Fc) = 0.37 V vs SSCE (0.1 M TBAH/CH$_3$CN)—and ferrocene is stable and unreactive in solution. While FcPF$_6$ is paramagnetic, ferrocene exhibits a sharp singlet at δ 4.10 ppm in acetonitrile where no signals from the Ir complex occur, thus making it a good indicator that oxidation has transpired.

(28) (a) Bushnell, G. W.; Decker, M. J.; Eadie, D. T.; Stobart, S. R.; Vefghi, R. *Organometallics* **1985**, *4*, 2106. (b) Cotton, F. A.; Poli, R. *Organometallics* **1987**, *6*, 1743. (c) Wu, J.; Reinking, M. K.; Fanwick, P. E.; Kubiak, C. P. *Inorg. Chem.* **1987**, *26*, 247.

(29) Baird, M. C. *Prog. Inorg. Chem.* **1968**, *9*, 1.

Table VIII. Selected Bond Angles (deg) for $[Ir(CO)(P(p\text{-tol})_3)(mnt)]_2$[a]

C9–Ir1–S1	93.6 (3)	C5–S3–Ir2	101.9 (4)
C9–Ir1–S2	164.0 (3)	C6–S4–Ir2	102.1 (4)
C9–Ir1–P2	99.1 (3)	C6–S4–Ir1	107.9 (3)
C9–Ir1–S4	92.9 (3)	Ir2–S4–Ir1	69.81 (8)
C9–Ir1–Ir2	108.7 (3)	C21–P1–C31	107.4 (4)
S1–Ir1–S2	88.2 (1)	C21–P1–C11	104.8 (4)
S1–Ir1–P2	95.5 (1)	C21–P1–Ir2	113.8 (3)
S1–Ir1–S4	156.9 (1)	C31–P1–C11	104.5 (4)
S1–Ir1–Ir2	102.45 (8)	C31–P1–Ir2	108.2 (3)
S2–Ir1–P2	96.5 (1)	C11–P1–Ir2	117.3 (3)
S2–Ir1–S4	79.6 (1)	C61–P2–C51	106.9 (5)
S2–Ir1–Ir2	55.41 (7)	C61–P2–C41	104.6 (4)
P2–Ir1–S4	105.4 (1)	C61–P2–Ir1	115.4 (4)
P2–Ir1–Ir2	145.52 (7)	C51–P2–C41	104.3 (5)
S4–Ir1–Ir2	54.47 (7)	C51–P2–Ir1	107.2 (3)
C10–Ir2–S3	94.2 (3)	C41–P2–Ir1	117.5 (3)
C10–Ir2–S4	161.5 (3)	C2–C1–C3	119 (1)
C10–Ir2–P1	97.2 (3)	C2–C1–S1	125.0 (8)
C10–Ir2–S2	91.1 (3)	C3–C1–S1	115.6 (8)
C10–Ir2–Ir1	105.9 (3)	C4–C2–C1	120 (1)
S3–Ir2–S4	88.7 (1)	C4–C2–S2	119.2 (8)
S3–Ir2–P1	100.4 (1)	C1–C2–S2	120.5 (8)
S3–Ir2–S2	158.2 (1)	N1–C3–C1	179 (1)
S3–Ir2–Ir1	103.69 (9)	N2–C4–C2	178 (1)
S4–Ir2–P1	100.3 (1)	C6–C5–C8	117 (1)
S4–Ir2–S2	79.9 (1)	C6–C5–S3	125.9 (9)
S4–Ir2–Ir1	55.72 (7)	C8–C5–S3	117 (1)
P1–Ir2—S2	99.8 (1)	C5–C6–C7	123 (1)
P1–Ir2–Ir1	144.96 (7)	C5–C6–S4	121.3 (8)
S2–Ir2–Ir1	54.57 (7)	C7–C6–S4	115.9 (9)
C1–S1–Ir1	102.9 (11)	N3–C7–C6	177 (1)
C2–S2–Ir1	103.3 (3)	N4–C8–C5	177 (2)
C2–S2–Ir2	110.6 (3)	O1–C9–Ir1	178 (1)
Ir1–S2–Ir2	70.02 (8)	O2–C10–Ir2	177 (1)

[a] Estimated standard deviations in the least significant figure are given in parentheses.

significantly longer than the Ir–S(chelate) distance. The Ir–S(chelate) bonds are all longer than those for the Ir(I)–S(mnt) bonds in the charge-transfer complex discussed above and shorter than those reported for Ir(III)–S bonds.[21,22] This supports the formal assignment of the Ir atoms to a 2+ oxidation state. The other bond distances within the mnt ligand are in good agreement with previously reported values.[21-23] The Ir–P bond lengths, 2.348 (3) and 2.362 (3) Å, are in agreement with those for Ir–P bonds,[21,22,24,30] which range from 2.28 to 2.40 Å.

In solution, $[Ir(CO)(P(p\text{-tol})_3)(mnt)]_2$ exhibits spectroscopic properties consistent with those of the structure in the solid. In the ^1H NMR spectrum, three resonances are observed: a singlet at δ 1.94, a doublet at δ 6.91, and a doublet of doublets at δ 7.28 corresponding to the tolyl methyl protons, the ortho phenyl protons and the meta phenyl protons, respectively. A single sharp singlet is found at δ −17.99 in the ^{31}P NMR spectrum. The mnt ligand exhibits two ν_{CN} bands at 2204 (m) and 2227 (w) cm^{-1}.[31] These data are consistent with electronically and structurally equivalent Ir centers.

Photoinduced Electron Transfer. Acetonitrile solutions of $Ir(P(OPh)_3)_2(mnt)^-$ (**2**) and MV^{2+} in the dark give rise to a new charge transfer band at 532 nm as shown in Figure 8. This broad featureless absorbance appears on the low-energy tail of the lowest energy band of **3** and corresponds to E_{op} of the CT complex $[MV^{2+}, IR(P(OPh)_3)_2(mnt)^-]$. The extinction coefficient, ϵ_{AD},

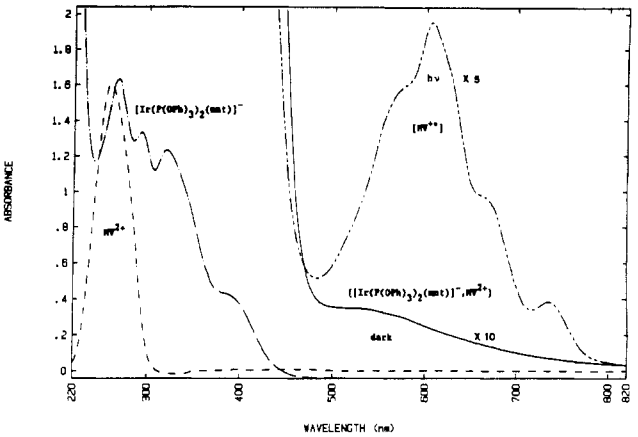

Figure 8. UV/visible spectra in acetonitrile solution: (a) TBA[Ir(P(OPh)$_3$)$_2$(mnt)] (-·-); (b) $MV(PF_6)_2$ (---); (c) TBA[Ir(P(OPh)$_3$)$_2$(mnt)] + $MV(PF_6)_2$ (—) in the dark; (d) solution from part c after photolysis with 350–500-nm light for 30 min (-···-). The scale in part c is 10 and that in part d is 5 times that of parts a and b.

for this band and the ion-pair association constant, K_{AD}, were determined as described above for the dicarbonyl complex and are 300 ± 35 cm^{-1} M^{-1} and 11 ± 3 M^{-1}. The magnitudes of K_{AD} and ϵ_{AD} are similar to those obtained for the dicarbonyl case. Again, there appears to be a slight concentration dependence on [Ir(I)]—ϵ_{AD} and K_{AD} = 345 cm^{-1} M^{-1} and 13 M^{-1} at 1 mM and 286 cm^{-1} M^{-1} and 8.1 M^{-1} at 10 mM.

At noted above, solutions of $[Ir(CO)_2(mnt)]^-$ and MV^{2+} gave the same UV/visible spectrum under N_2 or O_2 whether in the dark or upon photolysis. By contrast, nitrogen- or vacuum-degassed acetonitrile solutions containing $Ir(P(OPh)_3)_2(mnt)^-$ and MV^{2+} that were photolyzed by using a medium-pressure Hg arc lamp and a 350–500-nm band-pass filter (corresponding to photolysis into the lowest energy absorption of the Ir(I) complex) yielded the methyl viologen radical cation ($MV^{\bullet+}$). Typical irradiation times were on the order of 30 min and led to a $MV^{\bullet+}$ concentration corresponding to 15–20% oxidation of the Ir(I) starting material. However, even upon prolonged irradiation (≥4 h), no further $MV^{\bullet+}$ was formed. When the solutions were placed in the dark, the $MV^{\bullet+}$ absorbance decayed as a function of time to ≤5% $MV^{\bullet+}$. This procedure was repeated seven times over a period of several days. After four photolysis cycles, a tan precipitate was observed to form in the bottom of the UV/visible cell but this did not appear to interfere with the photolysis reaction or the resultant change in the intensity of the $MV^{\bullet+}$ absorbance.

While the color change of MV^{2+} to $MV^{\bullet+}$ appeared to be reversible, the entire system was slowly decomposing, most probably via irreversible oxidation of the Ir(I) complex. While the oxidized Ir product may relate to the $[IrL(CO)(mnt)]_2$ dimer described above, further study is in progress to elucidate the nature of this product unequivocally.

Ir(I/II) Reorganization Energy in the IrLL′(mnt)$^-$ Systems. In outer-sphere electron transfer, the activation energy relates directly to the reorganization energy, which in turn depends on individual reorganization energies of oxidant and reductant. For the IrLL′(mnt)$^-$ complexes studied here, both the irreversible oxidation waves and the different coordination geometries preferred by Ir(I) and Ir(II) suggest a large reorganization energy for the Ir(I/II) couple. It is possible to obtain an estimate of this value based on the observed optical charge transfer band and eq 1. Of the systems exhibiting E_{op}, that of $Ir(P(OPh_3)_2(mnt)^-/MV^{2+}$ offers the best opportunity for analysis since the optical-charge-transfer band seen at 532 nm (Figure 8) is well-defined.

While the irreversibility of the Ir(I/II) oxidation waves precludes a determination of $E_{1/2}$ values for the different IrLL′(mnt)$^-$ complexes, it is clear that (1) $Ir(CO)(CN)(mnt)^{2-}$ is reducing enough to take MV^{2+} to $MV^{\bullet+}$ quantitatively, (2) $Ir(CO)_2(mnt)^-$ is too weakly reducing to generate any $MV^{\bullet+}$ in solutions of the Ir(I) complex with MV^{2+} under any of the conditions examined, and (3) the potential range spanned by the IrLL′(mnt)$^-$ complexes

(30) (a) Bellon, P. L.; Demartin, F. M.; Manassero, M.; Sansoni, M. *J. Organomet. Chem.* **1978**, *157*, 209. (b) Tulip, T. H.; Ibers, J. A. *J. Am. Chem. Soc.* **1979**, *101*, 4201. (c) Alexander, B. D.; Johnson, B. J.; Johnson, S. M.; Boyle, P. D.; Kann, N. C.; Mueting, A. M.; Pignolet, L. H. *Inorg. Chem.* **1987**, *26*, 3506. (d) Bleeke, J. R.; Peng, W.-J. *Organometallics* **1987**, *6*, 1576. (e) Egan, J. W.; Hughes, R. P.; Rheingold, A. L. *Organometallics* **1987**, *6*, 1578. (f) Burk, M. J.; Segmuller, B.; Crabtree, R. H. *Organometallics* **1987**, *6*, 2241.

(31) This dual mnt CN stretch has also been seen for the alkylated mnt in ref 23a and in $Ir(CH_2CH_2CH_2\text{-mnt})(CO)(P(p\text{-tol})_3)$: Bradley, P.; Eisenberg, R. Unpublished results.

is ~0.35 V (see Table IV). While the lack of $E_{1/2}$ values obviates calculation of ΔE_0 for electron transfer between $Ir(P(OPh)_3)_2(mnt)^-$ and MV^{2+}, we can estimate that for this system ΔE_0 is ~-0.1 v based on the fact that the slightly more reducing complex $Ir(CO)(PPh_3)(mnt)^-$ produces partial reduction of MV^{2+} thermally. The error on this estimate of ΔE_0 is sizable but leads to only small changes in the reorganization energy estimated by using eq 1.

The reorganization energy λ obtained by using E_{op} of 532 nm and ΔE_0 of -0.1 V is 56 kcal/mol. While λ is a composite of several terms, the two dominant ones are the individual reorganization energies of the reaction components. From the self-exchange rate constant for $MV^{2+/+\cdot}$,[7c,32] it is possible to estimate $\lambda(MV^{2+})$ as 12-16 kcal/mol, leaving λ for the Ir(I/II) couple in this system as 40-44 kcal/mol. This value is consistent with the notion of a large reorganization energy in the oxidation of these $IrLL'(mnt)^{n-}$ systems.

Conclusions. The results presented here show that as ligand donor ability is changed in the $IrLL'(mnt)^{n-}$ system, the reducing ability of the complex is systematically altered. This reveals itself by different electron-transfer behavior with the acceptor molecule MV^{2+}. The most reducing complex, $Ir(CO)(CN)(mnt)^{2-}$, reduces MV^{2+} quantitatively by thermal electron transfer while the least reducing complex, $Ir(CO)_2(mnt)^-$, exhibits only an optical-charge-transfer band without formation of free $MV^{+\cdot}$. The complexes $Ir(CO)(PPh_3)(mnt)^-$ and $Ir(P(OPh)_3)_2(mnt)^-$ show intermediate behavior with photoassisted and photoinduced electron transfer, respectively. From E_{op} of the last of these complexes with MV^{2+}, it is possible to estimate the reorganization energy of the Ir(I/II) couple in this complex as 40-44 kcal/mol. The X-ray structural results show that oxidation of $Ir(CO)(P(p\text{-tol})_3)(mnt)^-$ leads to dimerization and a structure containing an Ir-Ir single bond with a coordination geometry for Ir(II) that is strikingly different from the square-planar arrangement usually seen for Ir(I).

Acknowledgment. We wish to thank the National Science Foundation (Grant CHE 86-03055) for support of this work, and the Johnson Matthey Co., Inc., for a generous loan of iridium salts. We also wish to acknowledge assistance from Dr. Gordon S. Miller in early stages of this work and helpful discussions with Prof. George McLendon.

Supplementary Material Available: Table SI (complete crystal data and intensity collection parameters for the structure determinations of **5** and **6b**), Tables SII and SIII (refined thermal parameters and calculated hydrogen positional parameters for **5**), Tables SIV-SVII (refined thermal parameters, calculated hydrogen positional parameters, and complete bond distances and angles for **6b**), and Figure S1 (crystal structure packing for **6b**) (15 pages); tables of observed and calculated structure factor amplitudes (×10) for **5** and **6b** (44 pages). Ordering information is given on any current masthead page.

(32) Bock, C. R.; Connor, J. A.; Gutierrez, A. R.; Meyer, T. J.; Whitten, D. G.; Sullivan, B. P.; Nagle, J. K. *Chem. Phys. Lett.* **1979**, *61*, 522.

Contribution from the Departments of Chemistry, Indiana University, Bloomington, Indiana 47405, and University of Oslo, Blindern, N-0315, Oslo 3, Norway

Structure and Reactivity of $Cr(OCMe_3)_4$

Eric G. Thaler,[†] Kristin Rypdal,[‡] Arne Haaland,*[,‡] and Kenneth G. Caulton*[,†]

Received October 20, 1988

$Cr(O^tBu)_4$ has been characterized by ^1H NMR and magnetic susceptibility methods, and the structure has been determined in the gas phase. The gas-phase electron diffraction pattern recorded with a nozzle temperature of about 130 °C is consistent with a model of S_4 symmetry. The most important structural parameters are Cr-O = 175.1 (7) pm, O-C = 141.1 (12) pm, and C-C = 151.7 (7) pm and ∠CrOC = 142 (2)° and ∠OCC = 107.8 (4)°. No evidence is found for deviation from tetrahedral valence angles at Cr. $Cr(O^tBu)_4$, in which chromium is completely shielded by a hydrocarbon exterior, shows no tendency to add the Lewis bases PMe_2Ph, PPh_2H, MeCN, MeNC, or CO but oxidizes $LiPPh_2$ to Ph_2PPPh_2, with production of $LiCr(O^tBu)_4$. Several one-electron redox reagents containing open coordination sites will interconvert $Cr(O^tBu)_4^-$ and $Cr(O^tBu)_4$, with evidence that each proceeds by an inner-sphere mechanism.

Introduction

$Cr(O^tBu)_4$ was initially reported by Hagihara and co-workers in 1959 and was the first monomeric Cr(IV) species supported solely by organic ligands.[1] Its synthesis was somewhat unique for metal alkoxides in that it may be considered formally as an oxidative addition of 2 equiv of di-*tert*-butyl peroxide to the Cr^0 metal center of bis(benzene)chromium. This first report was followed by the report of several alternative synthetic routes to $Cr(O^tBu)_4$,[2] a brief summary of some of its reaction chemistry (which emphasized proton-transfer reactions),[3] and a report on the thermodynamics of this compound.[4] Characterization of $Cr(O^tBu)_4$ includes solid-state magnetic susceptibility measurements, elemental analysis, and a cryoscopic molecular weight determination. Infrared, electronic, and ESR spectra were consistent with the compound having approximate T_d symmetry in solution. However, band splitting in the ligand field spectrum was interpreted as evidence for a distortion from tetrahedral symmetry to D_{2d}. Due to the high volatility of this compound, we felt that a more exact structural characterization could be accomplished through a gas-phase electron diffraction study, where the $Cr(O^tBu)_4$ molecules would be devoid of the solvent interactions possible in solution spectral studies, and no crystal packing forces would be present, as can be the case in X-ray structural analysis. We report here the results of such a study and present some of the reactivity trends for $Cr(O^tBu)_4$.

Experimental Section

General Procedures. All operations were performed under N_2 (unless specifically stated otherwise) by using standard Schlenk techniques for handling air- and moisture-sensitive materials. Tetrahydrofuran, benzene, and toluene were all dried and distilled prior to use from solutions containing sodium/potassium benzophenone ketyl. "Ultra-high-purity" grade hydrogen and carbon monoxide gases were purchased from Air Products. Copper(I) chloride was synthesized by literature methods,[5] as was $CrCl_3(THF)_3$.[6]

[†] Indiana University.
[‡] University of Oslo.

(1) Hagihara, M.; Yamasaki, H. *J. Am. Chem. Soc.* **1959**, *81*, 3160.
(2) Basi, J. S.; Bradley, D. C. *Proc. Chem. Soc.* **1963**, 305. Krauss, H. L.; Munster, G. *Z. Anorg. Allg. Chem.* **1967**, *24*, 352. Alyea, E. C.; Basi, J. S.; Bradley, D. C.; Chisholm, M. H. *Chem. Commun.* **1968**, 495.
(3) Alyea, E. C.; Basi, J. S.; Bradley, D. C.; Chisholm, M. H. *J. Chem. Soc.* **1971**, 772.
(4) Bradley, D. C.; Hillyer, M. J. *Trans. Faraday Soc.* **1966**, *62*, 2382.
(5) *Inorg. Synth.* **1946**, *2*, 1.
(6) Herwig, W.; Zeiss, H. H. *J. Org. Chem.* **1958**, *23*, 1404.

0020-1669/89/1328-2431$01.50/0